Smart Materials and Structures

PAPER

High out-of-plane deformation cone dielectric elastomer actuator via partitioned applied voltage

To cite this article: Yaguang Guo *et al* 2025 *Smart Mater. Struct.* **34** 085029

IOP Publishing Smart Materials and Structures
Smart Mater. Struct. **34** (2025) 085029 (9pp) https://doi.org/10.1088/1361-665X/adfbb5

High out-of-plane deformation cone dielectric elastomer actuator via partitioned applied voltage

Yaguang Guo[1], **Liwu Liu**[2,*], **Yanju Liu**[2,3,*] **and Jinsong Leng**[4]

[1] School of Materials Science and Engineering, Harbin Institute of Technology (Shenzhen), Shenzhen 518055, People's Republic of China
[2] Department of Astronautical Science and Mechanics, Harbin Institute of Technology (HIT), PO Box 301, No. 92 West Dazhi Street, Harbin 150001, People's Republic of China
[3] Suzhou Research Institute, Harbin Institute of Technology, Suzhou 215100, People's Republic of China
[4] Center for Composite Materials and Structures, Science Park of Harbin Institute of Technology (HIT), PO Box 3011, No. 2 YiKuang Street, Harbin 150080, People's Republic of China

E-mail: liulw@hit.edu.cn and yj_liu@hit.edu.cn

Received 21 May 2025, revised 11 August 2025
Accepted for publication 14 August 2025
Published 29 August 2025

Abstract

The cone dielectric elastomer actuator (CDEA), which generates out-of-plane axisymmetric deformation under the action of electric field and mechanical force, has attracted a lot of attention and can be used in the design of soft robots. In this work, a novel method to increase its out-of-plane displacement is proposed. The ring-shaped electrode is divided into inner and outer parts, and voltages are applied separately. Experimental results show that this method can effectively improve the out-of-plane displacement. A theoretical model is developed to reveal the mechanism of the method and the theoretical results agree well with the experimental results. The influence of the initial voltage and area of the inner electrode on the out-of-plane displacement is analyzed. Furthermore, a CDEA-based pump module is developed to verify the applicability of the method.

Supplementary material for this article is available online

Keywords: dielectric elastomer actuator, theoretical model, pump module, out-of-plane deformation

1. Introduction

Dielectric elastomers (DEs) deform when stimulated by an external electric field. Due to the characteristics of fast responses, large deformation, lightweight, and cost-effectiveness, DE has been recently intensively explored and developed to a variety of structures with diverse functions [1–4], such as energy harvesters [5, 6], wearable soft communicators [7, 8], biomimetic soft lenses [9, 10], flying microrobots [11], soft robots [12–14], swimming robots [15, 16], etc.

The cone dielectric elastomer actuators (CDEAs), which can generate out-of-plane axisymmetric deformation, have been used in the design of swimming robots [17, 18], walking robots [19], pumps [20, 21], etc. Generally, a linear spring is used to apply a bias force to the DE film. When CDEA produces out-of-plane deformation, under the action of voltage, the linear spring extends, resulting in a reduction in the force exerted on the DE film. Consequently, displacement of CDEA is relatively small compared to applying a constant bias force to the DE film.

* Authors to whom any correspondence should be addressed.

To increase the out-of-plane displacement of CDEA, researchers have modified the bias system, replacing the simple linear spring with more complex mechanisms, such as a system consisting of linear bias spring and negative-rate bias spring [22], a pair of magnets [17], or a diamond four-bar mechanism [23]. These modifications help maintain or even increase the bias force during deformation. In addition, setting CDEA in an antagonistic configuration can further boost their out-of-plane displacement [20, 21]. By adjusting the frequency of the applied voltage, CDEA would also produce more significant out-of-plane displacement under resonance conditions [20].

Several theories [24–26] have been proposed to explain the nonlinear deformation mechanisms of CDEAs. When the DE film deforms out-of-plane under the action of the voltage and the bias force, the distribution of stretch and stress on the DE film near the disk is the largest. When the voltage applied on the DE film reaches a certain level, the stress in the latitude direction will be negative. Generally, the DE film is considered to be unable to withstand compressive stress, leading to the formation of wrinkles at the inner boundary of the ring-shaped electrode, which then gradually spread outward. This phenomenon is regarded as a typical failure mode of DE actuators, known as loss of tension. Further increases in voltage can cause the DE film to become more susceptible to electrical breakdown.

Up to now, most of the research pay attention to the bias systems that apply mechanical force to the DE film to increase the out-of-plane displacement of CDEA. The theoretical analysis reveals that if the applied bias force is constant, the deformation is limited by the failure mode of electrical breakdown or loss of tension at the inner boundary of the ring-shaped electrode. Due to the inhomogeneity of out-of-plane deformation, the film near the inner boundary of the ring-shaped electrode has failed, while a large part of the film near the outer boundary has almost no electro-induced deformation. Based on these insights, this work proposes a novel approach to increase the out-of-plane displacement of CDEA by applying a higher voltage specifically to the outer region of the film. The method was verified through experiments. A theoretical model was also developed to explain the mechanism of increasing out-of-plane displacement. According to the theoretical model, the influence of the area and initial voltage of the inner ring-shaped electrode on the out-of-plane displacement is analyzed in detail. Furthermore, the effectiveness of this method has been confirmed through its implementation in a CDEA-based pump module.

2. Design and experiment

As illustrated in figure 1, the ring-shaped electrode of the CDEA is divided into inner and outer parts, and the two ring-shaped electrodes are applied with voltages, independently. This configuration allows the voltage applied to the outer ring-shaped electrode to be increased to a higher level, thereby enhancing the out-of-plane displacement.

The fabrication process of the CDEA with two parts ring-shaped electrodes is shown in figure 1(a). The DE film was equi-biaxially pre-stretched and fixed. Then, the mask was applied to both sides of the pre-stretched DE film, and the dividing line with a width of 1.4 mm was drawn using a marker pen. Conductive carbon grease (846–80G, MG chemicals) was subsequently painted on both sides of the dividing line. Finally, a polymethyl methacrylate frame with an inner radius of 42 mm and a disk with a radius of 14 mm were attached to the film. In order to eliminate the influence of the bias system, a constant bias force was applied to the film by attaching a 280 g weight.

In the experiment, a laser displacement sensor (HG-C1050, Panasonic) was employed to measure the out-of-plane displacement of CDEA, as indicated in figure 1(b). High voltage amplifiers with small size (EMCO A60P-5, Q80-5, XP power) were used to power the CDEA. During the displacement tests, the same voltages were applied to the inner and outer electrodes, and each voltage was maintained for 20 s with a step value of 0.5 kV until wrinkles appeared at the inner boundary of the ring-shaped electrode. To prevent electrical breakdown when a higher voltage was applied to the outer electrode, the voltage of the inner ring-shaped electrode was fixed to the stable voltage when there were no wrinkles at the inner boundary, and then the voltage of the outer ring-shaped electrode was gradually increased until wrinkles were generated at the inner boundary of either the inner or outer ring-shaped electrodes. The measurement was repeated three times for each test condition to obtain the average value.

3. Computational model and method

As shown in figure 2, the DE film thickness is H in reference state. Then, the film is pre-stretched λ_{pre} and fixed on a frame with an inner radius b. A disk with a radius a is attached to the center and subjected to the force to generate axisymmetric out-of-plane deformation. Considering two adjacent material particles located at R and $R+dR$, they take the positions at $(r(R), z(R))$ and $(r(R+dR), z(R+dR))$, respectively in current state. The distance between two material particles is $dl = \lambda_1 dR$, where λ_1 is the stretch along the longitude direction. Define θ as the angle between the horizontal direction and tangent direction at material particle R. Geometric relations require

$$\frac{dr}{dR} = \lambda_1 \cos\theta \tag{1}$$

$$\frac{dz}{dR} = -\lambda_1 \sin\theta \tag{2}$$

The stretch λ_2 along the latitude direction

$$\lambda_2 = \frac{r}{R}. \tag{3}$$

Under the action of constant force F, the CDEA is in equilibrium. The force balance in z-direction and latitudinal direction, respectively, yields

$$\frac{d(Rs_1 \sin\theta)}{dR} = 0 \tag{4}$$

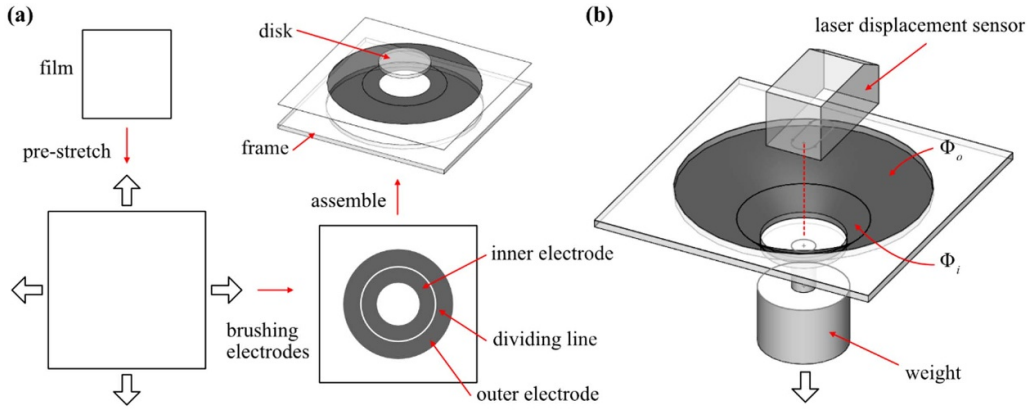

Figure 1. Schematic diagram of (a) fabrication process and (b) testing device of CDEA.

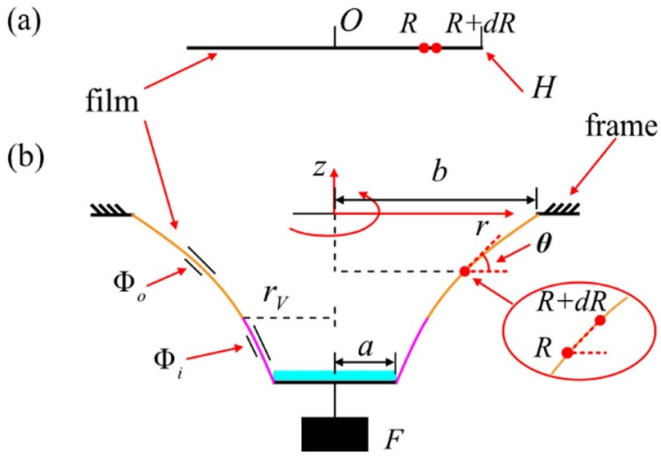

Figure 2. The cross-section of CDEA. (a) The film is in the reference state. (b) The CDEA deforms out-of-plane under the action of voltages and constant force in the current state.

$$\frac{d\left(Rs_1\cos\theta\right)}{dR}-s_2=0 \tag{5}$$

and

$$2\pi RHs_1\sin\theta-F=0 \tag{6}$$

where s_1 is the longitudinal nominal stress and s_2 is the latitudinal nominal stress. Combining equations (4) and (5), we can get

$$\frac{d\theta}{dR}=-\frac{s_2}{s_1R}\sin\left(\theta\right) \tag{7}$$

$$\frac{d\lambda_1}{dR}=\frac{s_2\cos\theta-s_1-R\frac{ds_1}{d\lambda_2}\frac{d\lambda_2}{dR}}{R\frac{ds_1}{d\lambda_1}}. \tag{8}$$

The stretch along the thickness direction can be written as $\lambda_3=1/\left(\lambda_1\lambda_2\right)$, where the material is taken to be incompressible. When a voltage is applied on the DE film, the electric field can be expressed as

$$E=\Phi\lambda_1\lambda_2/H \tag{9}$$

where Φ is the voltage applied on the DE film. Here, we employed the model of ideal DE [27, 28]. In this model, the dielectric behavior of the material is independent of deformation, and the true electric displacement D is linear with the electric field E, such as $D=E\varepsilon$, where ε is the permittivity of the material, considered as a constant. When the elastomer is subjected to both mechanical force and voltage, the stress can be expressed

$$\sigma_1=\lambda_1\frac{\partial W_{\mathrm{s}}\left(\lambda_1,\lambda_2\right)}{\partial\lambda_1}-\varepsilon E^2 \tag{10}$$

$$\sigma_2=\lambda_2\frac{\partial W_{\mathrm{s}}\left(\lambda_1,\lambda_2\right)}{\partial\lambda_2}-\varepsilon E^2 \tag{11}$$

where $W_{\mathrm{s}}(\lambda_1,\lambda_2)$ is the strain energy density of the DE. The nominal stress is related to the true stress by $s_1=\sigma_1/\lambda_1$ and $s_2=\sigma_2/\lambda_2$. The strain energy density is expressed by Gent model [29] to account for the strain stiffening effect of the DE material

$$W_{\mathrm{s}}\left(\lambda_1,\lambda_2\right)=-\frac{\mu J_{\mathrm{lim}}}{2}\log\left(1-\frac{\lambda_1^2+\lambda_2^2+\lambda_1^{-2}\lambda_2^{-2}-3}{J_{\mathrm{lim}}}\right) \tag{12}$$

where μ is the small-stress shear modulus, and J_{lim} is a constant reflecting the limiting stretch of the material. The ring-shaped electrode is divided into two parts from point V to the inner and outer parts to apply different voltages, namely

$$E=\begin{cases}\Phi_{\mathrm{i}}\lambda_1\lambda_2/H, & r_{\mathrm{a}}\leqslant r<r_{\mathrm{v}}\\ \Phi_{\mathrm{o}}\lambda_1\lambda_2/H, & r_{\mathrm{v}}\leqslant r\leqslant r_{\mathrm{b}}\end{cases}. \tag{13}$$

Considering the continuity conditions at point V, both deformation and longitudinal stress are continuous, namely [30–32]

$$\begin{aligned}&r\left(V_{\mathrm{i}}^{+}\right)=r\left(V_{\mathrm{o}}^{-}\right),z\left(V_{\mathrm{i}}^{+}\right)=z\left(V_{\mathrm{o}}^{-}\right),\theta\left(V_{\mathrm{i}}^{+}\right)=\theta\left(V_{\mathrm{o}}^{-}\right),\\&s_1\left(V_{\mathrm{i}}^{+}\right)=s_1\left(V_{\mathrm{o}}^{-}\right).\end{aligned} \tag{14}$$

The boundary conditions are as follows

$$r(a)=a,r(b)=b,z(b)=0. \tag{15}$$

In the calculation, the dimensionless quantities: r/a, z/a, s_1/μ, s_2/μ, $F/(2\pi aH\mu)$, $\Phi/\left(H\sqrt{\mu/\varepsilon}\right)$; geometric parameters: $b/a=3$, $r_v/a=1.4$, $r_v/a=1.7$, $r_v/a=2$, $\lambda_{pre}=2.5$; material parameters: $H=1$ mm, $\varepsilon=3.98\times10^{-11}$ Fm^{-1} were used [31]. In addition, the parameters $\mu=25.1$ kPa and $J_{lim}=270$ were adjusted to best fit the experimental data [26, 33]. Equations (1), (7) and (8) form a set of first-order differential equations. The differential equations are solved by shooting method according to the boundary conditions of equation (15) and the continuity conditions of equation (14) to obtain the deformation of the CDEA. The initial value θ is adjusted until the solution satisfies the boundary conditions.

4. Results and discussion

The electromechanical behaviors of the CDEA were calculated based on the parameters. Figure 3 shows the configuration changes of the CDEA with $r_v/a=1.7$ under different voltages. The black line indicates the disk of the CDEA. In figure 3(a), the same voltages are applied to both inner and outer electrodes. Compared to the initial configuration ($\Phi=0$), the out-of-plane displacement of CDEA increases with the increase of voltage. Figure 3(b) illustrates that different voltages were applied to the inner and outer electrodes. Each voltage is represented by a different color to distinguish the deformation of the inner electrode part and the outer electrode part. In all configurations shown, the inner voltage was set to 5 kV. As the outer voltage increases from 5 kV to 6.5 kV, the out-of-plane displacement further increased.

In order to apply different voltages to the CDEA in the experiment, the inner and outer electrodes were separated by a narrow band without compliant electrodes. To verify the influence of the narrow-band area without voltage on the out-of-plane displacement of CDEA, an experiment was carried out in which the entire area of the CDEA was coated with compliant electrodes ($r_v/a=0$ was used during theoretical calculations). It can be seen from figure 4(a) that when the voltage exceeds 3 kV, the out-of-plane displacement of CDEA increases significantly. The experimental results agree well with the theoretical results. In addition, the difference between the experimental results of the entire area was coated with compliant electrodes and those with a narrow band without compliant electrodes is so small that the effect of the narrow-band area without voltage on the out-of-plane displacement of CDEA can be ignored. Therefore, the part of the narrow band without voltage was not considered in the theoretical calculations.

In the experiment where the entire area of the actuator was covered by the compliant electrodes, wrinkles appeared at the inner boundary of the electrode when the voltage reaches 5.5 kV, which is widely regarded as loss of tension of the DE actuators. To ensure that the CDEA was not subjected to electrical breakdown, the voltage of the inner electrode was fixed at 5 kV and then gradually increased the voltage of the outer electrode when different voltages were applied to the inner and outer electrodes of the CDEA. Figure 4(b) illustrates the variation of out-of-plane displacement with voltage. The dashed lines represent the experimental results, while the dash–dot lines represent the theoretical results. The increase in outer voltage leads to a further increase in displacement. When the voltage is increased to a certain level, wrinkles occurred at the inner boundary of the outer electrode, causing the actuator to fail in loss of tension, as shown in figure 5. Comparing the experimental and theoretical results, the changing trend shows consistency. However, at higher outer electrode voltages, the theoretical values tend to be lower than the experimental results. This discrepancy may be attributed to the Gent model employed in the theoretical analysis may not fully capture the electromechanical behavior under the highly nonlinear and inhomogeneous deformation. In addition, the viscoelasticity of the DE material was not considered in the theoretical model. Although the voltage was maintained long enough in the experiments to minimize time-dependent effects, viscoelastic responses may still have a noticeable impact due to increased strain amplitudes at higher voltage levels.

Although wrinkles were observed on the actuator at a voltage of 5.5 kV, its displacement was also recorded. It should be pointed out that in order to ensure that the CDEA does not experience electrical breakdown, the voltage was not maintained for a long time as other experiments. The results are presented in figure 6. When the voltages are applied separately, as indicated by the blue bar in figure 6, the outer voltages correspond to the voltage values shown in figure 4(b). According to the experimental results, when the voltage of the inner electrode is 5 kV, the out-of-plane displacement of CDEA can be increased by 58.2% ($r_v/a=1.4$) at most. It can also be increased by 19.4% ($r_v/a=1.7$) relative to the voltage of both inner and outer electrodes are 5.5 kV (loss of tension). This demonstrates that applying voltages separately to the inner and outer electrodes significantly improves the out-of-plane displacement of the CDEA.

The stretch and stress distributions are described in figure 7 when voltages are applied to the inner and outer electrodes respectively. In this case, the inner voltage of the CDEA with $r_v/a=1.7$ is also set to 5 kV. When the voltages of the inner and outer electrodes are the same, the stretch and stress are smooth curves, as shown by the red line in figure 7. The stretch distribution along the longitude direction near the disk is the largest and decreases monotonically towards the outer boundary, while the stretch along the latitude direction remains constant at the inner and outer boundary due to the fixed constraint and reaches a peak at a certain position in the middle, seen in figures 7(a) and (b). The stress along the longitude direction is always in a state of tension, while the stress along the latitude direction will be negative at the inner boundary of the ring-shaped electrode due to the increase in voltage, which will cause wrinkles and loss of tension at the inner boundary, seen in figures 7(c) and (d).

When the voltage of the inner electrode is fixed, and the voltage of the outer electrode is further increased, the stretch along the longitude direction will suddenly rise at the edge of voltage changes, followed by a gradual decrease. The stretch along the latitude direction would rise again due to the increase in voltage and then decrease after reaching the peak, as shown

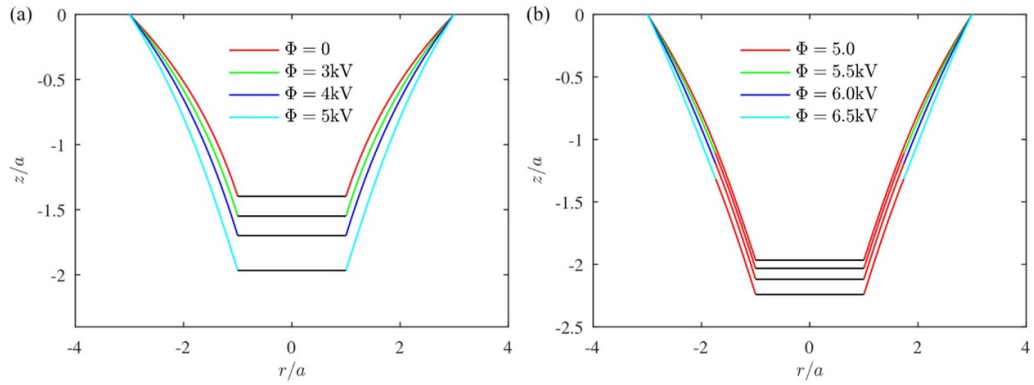

Figure 3. The configuration of the CDEA. (a) The same voltages are applied to the inner and outer electrodes. (b) The voltage of the inner electrode is fixed at 5 kV, and the voltage of the outer electrode is gradually increased to 6.5 kV.

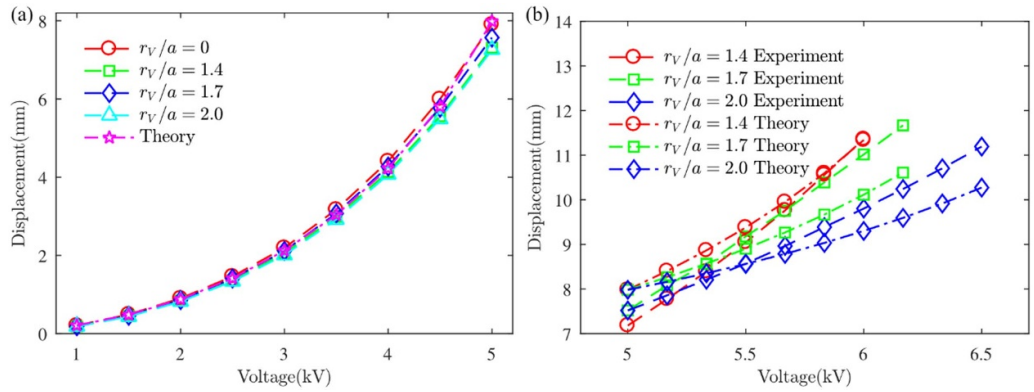

Figure 4. Comparison of theoretical and experimental results. (a) The same voltages are applied to the inner and outer electrodes. (b) The voltage of the inner electrode is fixed at 5 kV, and the voltage of the outer electrode is gradually increased until wrinkles occur.

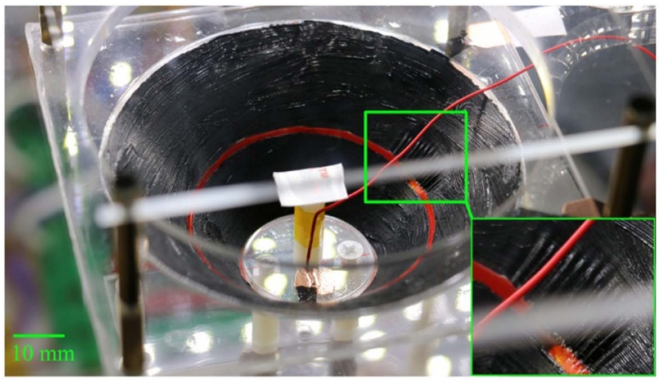

Figure 5. Photo of loss of tension when the inner and outer voltages are 5.0 kV and 6.3 kV respectively.

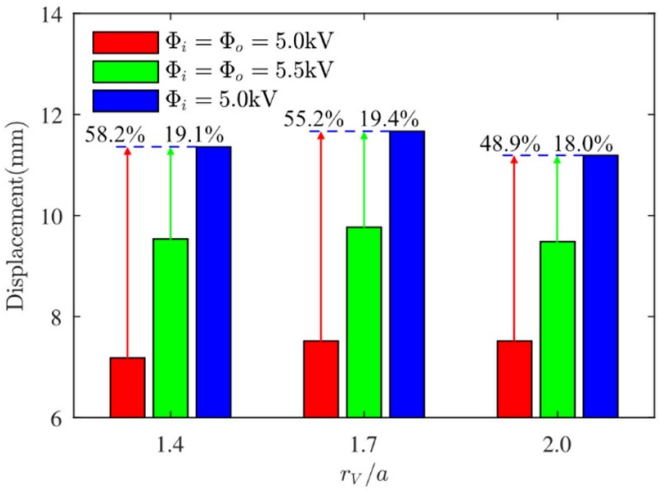

Figure 6. Comparison of displacement under different inner voltages.

in figures 7(a) and (b). The stress along the longitude direction is always positive, while the stress along the latitude direction suddenly drops due to the increase in voltage, followed by a gradual increase. The trends of the inner and outer ring-shaped electrodes under different voltages are consistent with the changing trends of all the same voltages.

The voltage of the inner electrode has a great influence on the out-of-plane displacement. Figure 8(a) shows the change in displacement as the voltage of the outer electrode and r_v/a increase when the voltage of the inner electrode is 5 kV. As the voltage of the outer electrode increases or r_v/a decreases, the displacement of CDEA gradually increases. The red line in figure 8 represents that the latitudinal stress of the inner boundary of the outer electrode is less than zero, and the actuator suffers loss of tension. In contrast, the blue line represents that

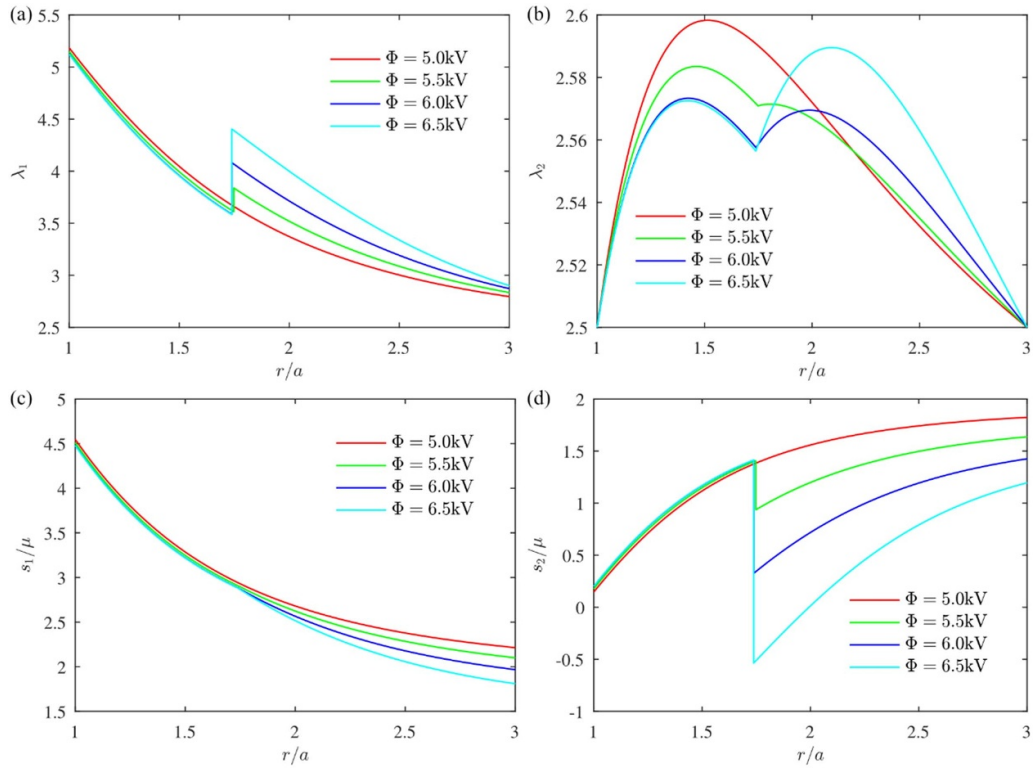

Figure 7. The distribution of stretch and stress. Figures (a) and (b) are stretches in the longitude and latitude directions, respectively. Figures (c) and (d) are stresses in the longitude and latitude directions, respectively.

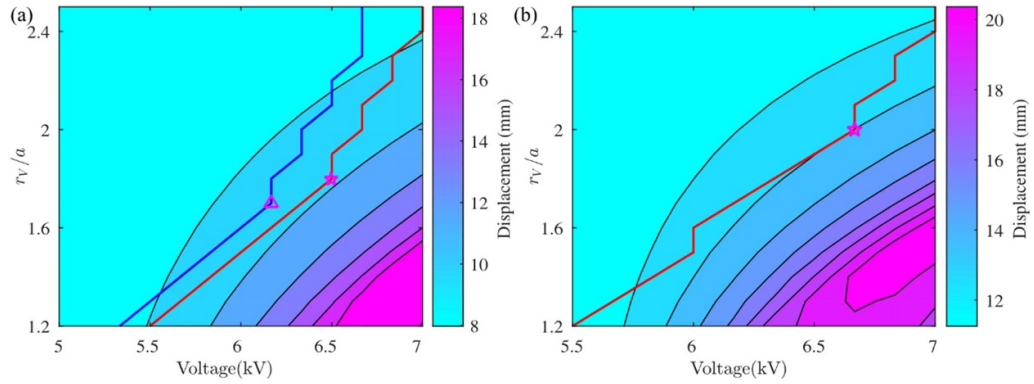

Figure 8. The influence of inner voltage and r_v/a on the out-of-plane displacement of CDEA. The initial voltage of the inner electrode is (a) 5 kV and (b) 5.5 kV, respectively. Where the red line denotes loss of tension, the blue line represents that when the inner boundaries of the inner and outer electrodes reach almost the same latitudinal stress and the mark represents the maximum value on the line.

when the inner boundaries of the inner and outer electrodes reach almost the same latitudinal stress. That is, the voltage below this line indicates a relatively safe operating range for the CDEA. The marked point on the line denotes the maximum displacement achieved. Compared with the voltages of both inner and outer electrode are 5 kV, the out-of-plane displacement can be increased by up to 32.9% ($r_v/a = 1.7$) when the voltage of the inner electrode is 5 kV, and the stress level of the inner boundary of the inner and outer electrodes is almost the same. Conversely, if the latitudinal stress at the inner boundary of the outer electrode is less than zero, the out-of-plane displacement can be increased by 40.5% ($r_v/a = 1.8$).

In figure 8(b), the voltage of the inner electrode is set to 5.5 kV, and the actuator has suffered loss of tension. When the r_v/a is small, the voltage of the outer electrode can only increase slightly, and loss of tension will occur due to the latitudinal stress of the inner boundary of the outer electrode is very small. As the r_v/a gradually increases, the voltage that the outer electrode can increase to a larger value, and the out-of-plane displacement also increase. If r_v/a continues to increase, the out-of-plane displacement will decrease again. When the voltage of the inner electrode is 5.5 kV, and the inner boundary latitudinal stress of the outer electrode is less than zero, the out-of-plane displacement can be increased by 20.3% ($r_v/a = 2$).

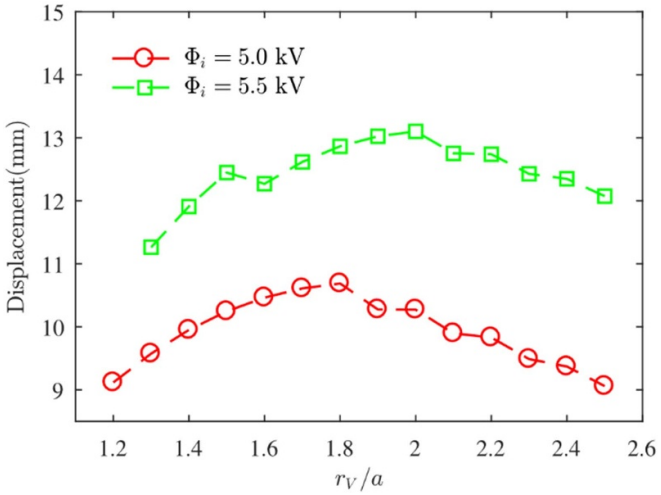

Figure 9. Effect of r_v/a on displacement when the voltage of the inner electrode is 5.0 kV or 5.5 kV.

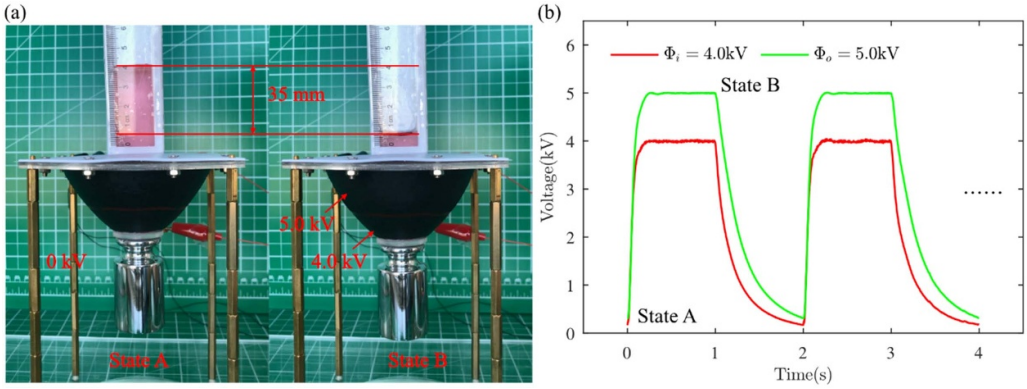

Figure 10. Demonstration of the pump module. (a) Photo of the pump module. (b) Actual voltages change with time when the inner and outer voltages are 4.0 kV and 5.0 kV respectively.

Figure 9 illustrates the maximum out-of-plane displacement that the CDEA can achieve (close to loss of tension) as r_v/a increases, under inner electrode voltages of 5 kV and 5.5 kV, respectively. It is observed that when r_v/a ranges between 1.8 and 2.0, the actuator exhibits more significant out-of-plane displacement. The discrepancy between theoretical predictions and experimental results can be attributed to several factors. First, due to the manual fabrication of the CDEA, unavoidable geometric and material inconsistencies are introduced. As the experiments progressed, the influence of viscoelastic effects, particularly stress relaxation, further decreased, resulting in a decrease in displacement over time. Moreover, when extracting the theoretical maximum displacement, the corresponding latitudinal stress is not always exactly zero, which may further contribute to the deviation. In summary, both theoretical and experimental results consistently demonstrate that the proposed method significantly enhances the out-of-plane displacement of the CDEA.

Here, the CDEA was also used as the driving structure of a pump module to verify the applicability of the method. As shown in figure 10(a), the 3D printed pump module component was assembled on the top of the CDEA. The cross-section dimensions of the part used to observe the height of the water level are 20 mm × 20 mm. A total of 150 ml of water was injected into the pump module and the water was colored by red ink for a clearer observation. When voltage is applied to the CDEA, its volume becomes larger and water will flow into the CDEA cause the water level to drop. In the experiment, a square wave voltage of 0.5 Hz was applied to the CDEA to simulate the working process instead of a quasi-static voltage. Figure 10(b) illustrates the actual voltages applied to the inner and outer electrodes. As shown in figure 10(a), it can be clearly seen that the water level has dropped significantly when the voltage is applied to the CDEA (i.e. from state A to state B).

The performance of the pump module under different voltages is shown in figure 11. When the inner voltage is set to 4.0 kV, the water level difference increased from 24 mm to 35 mm as the outer voltage increased from 4.0 kV to 5.0 kV. When the inner and outer voltages are both 4.5 kV, wrinkles have occurred at the inner boundary of the inner electrode. Therefore, this method can significantly improve the performance of the pump module.

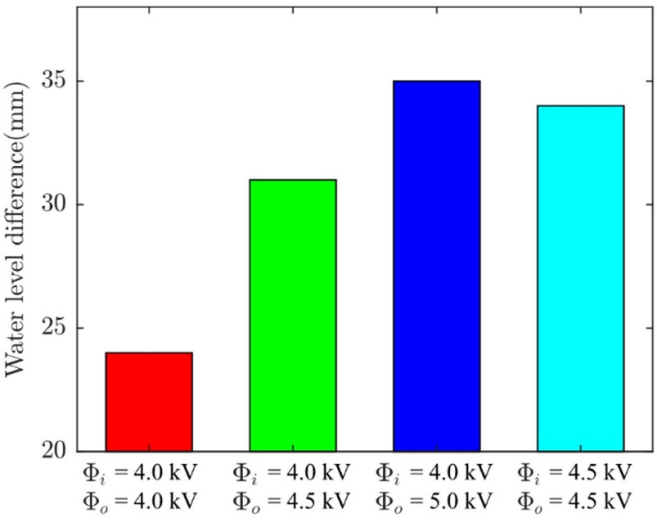

Figure 11. Performance of the pump module at different voltages.

5. Conclusion

In conclusion, a novel method for increasing the out-of-plane displacement of CDEA is proposed. The increase of the out-of-plane displacement is realized by dividing the actuation area of the CDEA into two parts and applying voltages separately. Experimental results show that this method can significantly improve the out-of-plane displacement of the actuator. When the voltage of the inner electrode is set to 5 kV, the out-of-plane displacement of CDEA can be increased by 58.2% ($r_v/a = 1.4$) at most. It can also be increased by 19.4% ($r_v/a = 1.7$) relative to the case where both the inner and outer electrodes are at 5.5 kV (loss of tension). A theoretical model was derived to reveal the mechanism of this method. The calculated results are in good agreement with the experimental results with adjusted parameters. Both the initial voltage and the occupied area of the inner electrode have significant effects on the out-of-plane displacement of the actuator. Furthermore, a pump module was developed to validate the applicability of the method. The water level difference of the pump module with an inner voltage of 4.0 kV increased from 24 mm to 35 mm when the outer voltage increased from 4.0 kV to 5.0 kV. These results will be beneficial to the development and application of CDEAs.

Data availability statement

All data that support the findings of this study are included within the article (and any supplementary files).

Acknowledgments

This work was supported by the China Postdoctoral Science Foundation (Grant No. 2023TQ0096) and the Self-Planned Task of Songjiang Laboratory, Harbin Institute of Technology (Grant No. SL20230101).

Author contributions

Yaguang Guo 0000-0003-3213-5471
Data curation (equal), Writing – original draft (equal)

Liwu Liu
Supervision (equal), Writing – review & editing (equal)

Yanju Liu 0000-0001-8269-1594
Project administration (equal), Supervision (equal), Writing – review & editing (equal)

Jinsong Leng 0000-0001-5098-9871
Project administration (equal), Writing – review & editing (equal)

References

[1] Lu T, Ma C and Wang T 2020 Mechanics of dielectric elastomer structures: a review *Extreme Mech. Lett.* **38** 100752
[2] Guo Y, Liu L, Liu Y and Leng J 2021 Review of dielectric elastomer actuators and their applications in soft robots *Adv. Intell. Syst.* **3** 2000282
[3] Gu G, Zhu J, Zhu L and Zhu X 2017 A survey on dielectric elastomer actuators for soft robots *Bioinspir. Biomim.* **12** 011003
[4] Sun W, Liang H, Zhang F and Li B 2022 Theoretical study of the electroactive bistable actuator and regulation methods *Int. J. Smart Nano Mater.* **14** 36–56
[5] Zhang C L, Lai Z H, Rao X X, Zhang J W and Yurchenko D 2020 Energy harvesting from a novel contact-type dielectric elastomer generator *Energy Convers. Manage.* **205** 112351
[6] Moretti G, Rosset S, Vertechy R, Anderson I and Fontana M 2020 A review of dielectric elastomer generator systems *Adv. Intell. Syst.* **2** 2000125
[7] Zhao H, Hussain A M, Israr A, Vogt D M, Duduta M, Clarke D R and Wood R J 2020 A wearable soft haptic communicator based on dielectric elastomer actuators *Soft Robot.* **7** 451–61
[8] Ji X, Liu X, Cacucciolo V, Civet Y, El Haitami A, Cantin S, Perriard Y and Shea H 2020 Untethered feel-through haptics using 18-μm thick dielectric elastomer actuators *Adv. Funct. Mater.* **31** 2006639
[9] Li J R, Wang Y, Liu L W, Xu S, Liu Y J, Leng J S and Cai S Q 2019 A biomimetic soft lens controlled by electrooculographic signal *Adv. Funct. Mater.* **29** 1903762
[10] Ghilardi M, Boys H, Torok P, Busfield J J C and Carpi F 2019 Smart lenses with electrically tuneable astigmatism *Sci. Rep.* **9** 16127
[11] Chen Y, Zhao H, Mao J, Chirarattananon P, Helbling E F, Hyun N-S P, Clarke D R and Wood R J 2019 Controlled flight of a microrobot powered by soft artificial muscles *Nature* **575** 324–9
[12] Ji X, Liu X, Cacucciolo V, Imboden M, Civet Y, Haitami A E, Cantin S, Perriard Y and Shea H 2019 An autonomous untethered fast soft robotic insect driven by low-voltage dielectric elastomer actuators *Sci. Robot.* **4** eaaz6451
[13] Li T, Zou Z, Mao G, Yang X, Liang Y, Li C, Qu S, Suo Z and Yang W 2018 Agile and resilient insect-scale robot *Soft Robot.* **6** 133–41
[14] Guo Y, Guo J, Liu L, Liu Y and Leng J 2022 Bioinspired multimodal soft robot driven by a single dielectric elastomer actuator and two flexible electroadhesive feet *Extreme Mech. Lett.* **53** 101720
[15] Li G *et al* 2021 Self-powered soft robot in the Mariana Trench *Nature* **591** 66–71

[16] Liu B, Chen F, Wang S, Fu Z, Cheng T and Li T 2017 Electromechanical control and stability analysis of a soft swim-bladder robot driven by dielectric elastomer *J. Appl. Mech.* **84** 091005
[17] Yang T *et al* 2018 A soft artificial muscle driven robot with reinforcement learning *Sci. Rep.* **8** 14518
[18] Tang C, Ma W, Li B, Jin M and Chen H 2019 Cephalopod-inspired swimming robot using dielectric elastomer synthetic jet actuator *Adv. Eng. Mater.* **22** 1901130
[19] Nguyen C T, Phung H, Nguyen T D, Jung H and Choi H R 2017 Multiple-degrees-of-freedom dielectric elastomer actuators for soft printable hexapod robot *Sens. Actuators A* **267** 505–16
[20] Cao C, Gao X and Conn A 2019 A magnetically coupled dielectric elastomer pump for soft robotics *Adv. Mater. Technol.* **4** 1900128
[21] Guo Y, Liu L, Liu Y and Leng J 2021 Antagonistic cone dielectric elastomer actuator: analysis, experiment and application *Extreme Mech. Lett.* **42** 101134
[22] Hodgins M, York A and Seelecke S 2013 Experimental comparison of bias elements for out-of-plane DEAP actuator system *Smart Mater. Struct.* **22** 094016
[23] Wang H-M, Zhu J-Y and Ye K-B 2009 Simulation, experimental evaluation and performance improvement of a cone dielectric elastomer actuator *J. Zhejiang Univ. Sci. A* **10** 1296–304
[24] He T, Zhao X and Suo Z 2009 Dielectric elastomer membranes undergoing inhomogeneous deformation *J. Appl. Phys.* **106** 083522
[25] He T, Cui L, Chen C and Suo Z 2010 Nonlinear deformation analysis of a dielectric elastomer membrane–spring system *Smart Mater. Struct.* **19** 085017
[26] Mao G, Wu L, Fu Y, Liu J and Qu S 2018 Voltage-controlled radial wrinkles of a trumpet-like dielectric elastomer structure *AIP Adv.* **8** 035314
[27] Suo Z 2010 Theory of dielectric elastomers *Acta Mech. Solida Sin.* **23** 549–78
[28] Zhao X and Suo Z 2007 Method to analyze electromechanical stability of dielectric elastomers *Appl. Phys. Lett.* **91** 061921
[29] Gent A N 1996 A new constitutive relation for rubber *Rubber Chem. Technol.* **69** 59–61
[30] Li J R, Lv X F, Liu L W, Liu Y J and Leng J S 2020 Computational model and design of the soft tunable lens actuated by dielectric elastomer *J. Appl. Mech.* **87** 071005
[31] Lu T, Cai S, Wang H and Suo Z 2013 Computational model of deformable lenses actuated by dielectric elastomers *J. Appl. Phys.* **114** 104104
[32] Koh S J A, Li T, Zhou J, Zhao X, Hong W, Zhu J and Suo Z 2011 Mechanisms of large actuation strain in dielectric elastomers *J. Polym. Sci. B* **49** 504–15
[33] Li T, Keplinger C, Baumgartner R, Bauer S, Yang W and Suo Z 2013 Giant voltage-induced deformation in dielectric elastomers near the verge of snap-through instability *J. Mech. Phys. Solids* **61** 611–28